# Reduced and mixed precision turbulent flow simulations using explicit finite difference schemes

Bálint Siklósi<sup>a,b,\*</sup>, Pushpender K. Sharma<sup>b</sup>, David J. Lusher<sup>c</sup>, István Z. Reguly<sup>a</sup>, Neil D. Sandham<sup>b</sup>

<sup>a</sup>Pázmány Péter Catholic University, Szentkirályi u. 28, Budapest, 1088, Hungary <sup>b</sup>University of Southampton, Boldrewood Campus, Burgess Rd, Southampton, SO16 7QF, United Kingdom <sup>c</sup>Japan Aerospace Exploration Agency (JAXA), 7-44-1 Jindaiji Higashi-machi, Chofu-shi, Tokyo, 182-8522, Japan

#### Abstract

The use of reduced and mixed precision computing has gained increasing attention in high-performance computing (HPC) as a The use of reduced and mixed precision computational efficiency, particularly on modern hardware architectures like GPUs. In this work, we explore the application of mixed precision arithmetic in compressible turbulent flow simulations using explicit finite difference schemes. We extend the OPS and OpenSBLI frameworks to support customizable precision levels, enabling fine-grained control over precision allocation for different computational tasks. Through a series of numerical experiments on the Taylor-Green vortex benchmark, we demonstrate that mixed precision stategies, such as half-ingle and single-double combinations, can offer significant performance gains without compromising numerical accuracy. However, pure half-precision computations result in unacceptable accuracy loss, underscoring the need for careful precision selection. Our results show that mixed precision configurations can reduce memory usage and communication overhead, leading to notable speedups, particularly on multi-GPU and multi-GPU systems.

\*\*Keywords:\*\* Floating point precision, Mixed precision, Computational fluid dynamics, Computational performance and scalability, OpenSBLI, OPS, GPU

1. Introduction

The advent of artificial intelligence has led to the widespread adoption of reduced precision formats in hardware such as half-precision (16-bit) floating-point arithmetic. While this transition presents opportunities for significant performance gains, it also raises concerns regarding the accuracy and stability of numerical results, particularly in high-performance computing (HPC) applications that are sensitive to precision. The challenge lies in determining the appropriate balance between precision and performance, as the demand for understand the properties of the precision deficiency continues to grow.

Existing mixed precision tec means to improve computational efficiency, particularly on modern hardware architectures like GPUs. In this work, we explore the

sparse LU factorization, eigenvalue solvers, and GMRES implementations. FluidX3D [7], a lattice Boltzmann CFD software, has explored mixed precision techniques, although it is limited to specific models and lacks flexibility in accommodating other simulation types. OpenFOAM [8], another popular CFD framework, with its recent update, compiles its code in single precision while employing double precision exclusively for its linear algebra solvers. This approach allows OpenFOAM

of finite difference solvers, in conjunction with the OPS [10] library—designed for structured mesh solvers—we demonstrate the capability to generate optimized codes for multi-GPU and multi-CPU environments. OpenSBLI facilitates the generation of optimized reduced/mixed precision implementations of OPS codes, enabling efficient computations across various hardware configurations.

The flexibility afforded by OpenSBLI allows users to customize the precision of datasets utilized in their simulations. This capability is particularly advantageous in scenarios where computational efficiency is paramount, necessitating a careful balance between precision and performance. In this study, we

<sup>\*</sup>Corresponding author. Email address: siklosi.balint@itk.ppke.hu (Bálint Siklósi)

present a series of tests conducted on a compressible Taylor-Green vortex simulation, which serves as a benchmark for evaluating the performance and accuracy of reduced precision computing. Our findings reveal that employing half, single, and double precision formats, as well as mixtures such as half-single and single-double, yields significant speedups without compromising the numerical accuracy of the results. Notably, only the half-precision runs exhibited numerically unsatisfactory outcomes, highlighting the critical importance of precision selection in computational simulations.

The main contributions of this work are as follows:

- Extended OPS for Mixed Precision: We have enhanced the OPS library to support mixed precision operations, allowing for improved computational efficiency in structured mesh solvers.
- Automated Mixed Precision Implementation in OpenS-BLI: We extended the OpenSBLI framework to automate
  the generation of mixed precision implementations, simplifying the integration of these strategies into existing
  workflows.
- Proposed Mixed Precision Algorithm: Our study introduces a mixed precision algorithm that optimally maintains work and residual arrays in lower precision, effectively balancing memory usage and computational accuracy.
- Accuracy Validation with Taylor-Green Vortex: We demonstrated that all configurations, except for pure half precision (HP), maintain acceptable accuracy levels when evaluated using the Taylor-Green vortex benchmark. Importantly, we found that the accuracy of the results is independent of various simulation parameters, such as Reynolds number and Mach number. Additionally, multiple numerical schemes are affected similarly across different precision levels; thus, while choosing the appropriate scheme remains a critical factor for achieving accurate results, its performance is consistent regardless of whether reduced precision is employed.
- Comprehensive Performance Analysis: We provided a
  detailed performance evaluation focusing on memory efficiency and communication overhead, showcasing significant speedups achieved through our mixed precision
  strategies without compromising result integrity.

The paper is structured as follows: Section 2 provides a detailed discussion of floating-point arithmetic, including an introduction to half precision and the potential risks associated with using reduced precision, such as loss of accuracy and numerical instability. We also introduce the OPS and OpenS-BLI frameworks, outlining their relevance to high-performance computing applications. Section 3 focuses on the algorithmic changes required to implement mixed precision strategies effectively within finite difference methods. Section 4 presents our testing and evaluation, starting with an introduction to the Taylor-Green vortex test case. We then assess the accuracy

of various precision configurations and subsequently analyze the performance, highlighting both the computational speedups and memory savings achieved with mixed precision. Finally, in Section 5, we discuss conclusions and future work, highlighting the potential of mixed precision techniques in larger and more complex applications, as well as improvements in half-precision performance and flexibility in the OPS framework.

# 2. Methodology / Background

# 2.1. Floating-Point Arithmetic in CFD Applications

Floating-point arithmetic is a critical component in computational fluid dynamics (CFD) applications, enabling the representation and manipulation of real numbers in a way that can accommodate a wide range of values. This section provides an overview of floating-point arithmetic, its operational mechanics, the risks associated with using insufficient precision, and a discussion on half precision.

# 2.1.1. Overview of Floating-Point Arithmetic

Floating-point numbers are represented in computers using a format that consists of three main components: the sign bit, the exponent, and the significand (or mantissa). This representation allows for the encoding of very large and very small numbers by scaling the significand with the exponent. The standard format for floating-point representation is defined by the IEEE 754 standard [11], which specifies several precision levels, including single precision (32 bits) and double precision (64 bits). In a typical floating-point representation, a number is expressed as:  $value = (-1)^{sign} \times significand \times 2^{exponent}$ . This format allows for efficient arithmetic operations such as addition, subtraction, multiplication, and division, which are fundamental in CFD simulations that require iterative calculations over vast datasets.

### 2.1.2. Dangers of Using Too Small Precision

Using insufficient precision in floating-point arithmetic can lead to significant computational errors, particularly in CFD applications where numerical stability is crucial. Key issues include:

- Round-off Errors: When calculations exceed the precision limit (caused by the fixed length of the mantissa), the results can become inaccurate due to rounding. This is particularly problematic in iterative methods where errors can accumulate and lead to divergent results. For examples, see [12].
- Overflow and Underflow: In floating-point arithmetic, numbers can exceed the maximum representable value (overflow) or fall below the minimum in absolute value (underflow). Both scenarios can lead to catastrophic failures in simulations, causing incorrect physical predictions.
- Loss of Significance: After converting to floating-point and subtracting two nearly equal numbers, significant

digits can be lost, resulting in a substantial relative error. This is known as catastrophic cancellation, which can severely affect the accuracy of CFD simulations. For examples, see [13]

These issues underscore the importance of selecting an appropriate precision level that balances computational efficiency with the accuracy required for the specific CFD application.

# 2.1.3. Half Precision Floating-Point Arithmetic

Half precision floating-point arithmetic (FP16) has recently gained significant traction in high-performance computing (HPC). The FP16 format, which utilizes 16 bits for numerical representation, strikes a balance between computational efficiency and memory usage, making it particularly well-suited for modern GPU architectures. Recent advancements in NVIDIA GPUs, such as the Volta and Ampere architectures, have introduced native support for FP16, enabling substantial performance improvements in various scientific computations. The use of FP16 can lead to remarkable speedups in computational tasks. For instance, one study [14] has demonstrated that employing mixed precision techniques, which leverage FP16 alongside higher precision formats like FP32 or FP64, can achieve speedups of up to 4 times in iterative refinement solvers. This is primarily due to the enhanced computational throughput provided by Tensor Cores in NVIDIA GPUs, which are optimized for half precision arithmetic. Additionally, research has shown that FP16 can significantly reduce memory bandwidth requirements, allowing for faster data transfers and improved overall performance in large-scale simulations [15]. However, the transition to half precision is not without challenges. The limited range and precision of FP16 can introduce numerical instability, particularly in operations that require high accuracy. Specifically, catastrophic cancellation can result in substantial relative errors, particularly in time-marching methods where small perturbations can accumulate.

To address these challenges, researchers have proposed various strategies, such as iterative refinement and scaling techniques, to enhance the accuracy of computations while leveraging the performance benefits of FP16. For example, recent work has shown that using a modified LU factorization can produce more numerically stable results, effectively mitigating the risks associated with limited precision formats [16]. These approaches illustrate that while FP16 offers significant advantages in terms of speed and efficiency, careful consideration of numerical stability is essential to maintain the integrity of computational results in FDM CFD applications. In addition to half precision (FP16), another format gaining attention is bfloat16 [17], which retains the exponent size of FP32 while reducing the significand to 7 bits. This design allows bfloat16 to maintain a similar dynamic range as FP32, making it particularly useful in deep learning applications where training stability is crucial. However, despite its advantages, bfloat16 still has limitations in terms of precision, which can lead to numerical instability in certain computational scenarios. Furthermore, there are even smaller floating-point formats in use, such as float8 [18] and other reduced precision types, but due to the challenges and

inaccuracies encountered with FP16, we do not advocate for going lower in precision.

#### 2.2. OPS Domain-Specific Library

The Oxford Parallel library for Structured mesh solvers (OPS) [10] is a domain-specific library designed to streamline the implementation of high-performance applications in structured mesh computations. OPS provides a high-level abstraction for stencil operations commonly used in numerical methods, allowing developers to focus on algorithm development without the complexities associated with low-level parallel programming. This abstraction significantly enhances the ease of use and maintainability of the code, which is particularly beneficial for researchers and practitioners in the field. A notable feature of OPS is its capability to handle multiple datasets, each of which can be assigned its own precision. This flexibility allows for efficient management of different numerical requirements within a single application, accommodating varying precision needs across datasets. By enabling developers to specify precision at the dataset level, OPS facilitates the creation of applications that can dynamically adapt to the precision requirements of different computations, optimizing performance while ensuring accuracy. OPS is designed with performance portability in mind, allowing applications to run efficiently across a range of hardware architectures, including CPUs and GPUs. This portability is achieved through a combination of automated code generation and optimization techniques that adapt to the specific features of the underlying hardware, ensuring that applications can leverage the full capabilities of diverse computing environments. Furthermore, OPS supports various programming models, including OpenMP, MPI, and CUDA, providing developers with the flexibility to choose the most suitable approach for their specific application and hardware configuration. Overall, OPS represents a powerful tool for simplifying the development of structured mesh applications. Its focus on ease of use, performance portability, and support for multiple programming models makes it an attractive option for researchers looking to implement efficient and scalable numerical methods in their computational workflows.

#### 2.3. OpenSBLI

OpenSBLI [9] is a complete code generation system for computational fluid dynamics that automatically generates OPS code starting from a compact description of the governing equations using subscript notation. It uses symbolic Python to expand the governing equations and carry out the subsequent discretisation, using high-order finite differences. The front end is used to define and expand the governing equations and constituent relations. It also defines all the boundary and initial conditions and sets all the run time parameters. This provides an effective implementation of the 'separation of concerns' work flow [19], whereby users focusing on the fluid dynamics can carry out most tasks from the python front end. Alternatively, numerical methods developers can work either in the OPSC code or in the OpenSBLI code generation, while

computer-science-based performance optimisations can be carried out in the OPS translator. The main applications of OpenS-BLI are direct numerical simulation (DNS) and large eddy simulation (LES) of compressible-flow problems involving transition to turbulence or fully-developed turbulence on structured grids.

An initial version (V1) of the software [20] demonstrated the code-generation concept for simple low-speed periodic flows and the benefits of the OPS code translation in being able to run efficiently on heterogeneous computing architectures. The project was restarted from a clean code base in [21], which led to the subsequent public code release in [9]. This version (V2) included shock capturing using Weighted Essentially Non-Oscillatory (WENO) and less dissipative Targeted Essentially Non-Oscillatory (TENO) schemes along with a greatly expanded set of boundary-conditions and application demonstrations, including shock-wave/boundary-layer interactions [21] and channel flow validation test cases [22]. This release also included generalised curvilinear geometries. The current release version of OpenSBLI is V3 [23]. Version 3 added multi-block mesh support, airfoil simulations, new numerical methods and filters, and various performance and efficiency improvements. Reduced-dimension I/O, partial reductions for spanwise averaging, and mixed-precision support were also added, via upgrades to both OpenSBLI and the OPS library. The combination of multi-block capability and new filter-based shock-capturing schemes [23] has led to new applications of implicit LES simulations of flow over airfoils, including state-of-the-art studies of airfoil buffet in the transonic flow regime [24, 25] that exploit large GPU-based machines to perform high-fidelity simulations on the order of  $N \sim 10^{10}$ mesh points.

# 2.3.1. Numerical Methods and Split Formulations of the Equations

The accuracy of low- and mixed-precision algorithms is assessed in this work in the context of the unsteady full-3D Navier-Stokes equations for a compressible Taylor-Green vortex problem described in Section 4.1. All simulations are performed using explicit 4th-order accurate non-dissipative central-differencing. Both the convective and diffusive parts of the Navier-Stokes equations are solved at 4th-order to maintain consistent spatial order throughout. Time-stepping is performed by a low-storage explicit 3rd-order Runge-Kutta scheme. Details of the implementation have previously been given in [9].

Depending partly on the magnitude of the Reynolds number, direct application of standard central derivative approximations to the Navier-Stokes equations can lead to numerical instabilities [26]. This is due to an accumulation of aliasing errors that occurs from discrete evaluation of the product between two or more terms within the non-linear convective derivatives. The lack of numerical robustness can also be linked to the failure of standard formulations to discretely preserve quadratic invariants such as global kinetic energy in the inviscid limit [27]. To alleviate these discretisation issues, convective terms of the base Navier-Stokes equations are routinely re-

formulated in modern CFD codes in what are known as split formulations. These alternative formulations of the governing equations have been reported to improve numerical robustness via reduced aliasing errors and preservation of certain invariant quantities [28].

Various split-forms are available in the literature [28]. They typically focus on the reformulation of non-linear convective derivative terms that take the general form

$$C = \frac{\partial \rho u_j \varphi}{\partial x_i},\tag{1}$$

where  $\varphi$  takes the value of  $(1, u_i, E)$ , for the continuity, momentum, and energy components of the Navier-Stokes equations, respectively. As an example of one of the split-forms available in OpenSBLI, the Feiereisen quadratic split-form [29], expands these terms quadratically as

$$\frac{\partial \rho u_j \varphi}{\partial x_j} \to \frac{1}{2} \frac{\partial \rho u_j \varphi}{\partial x_j} + \frac{1}{2} \left( \varphi \frac{\partial \rho u_j}{\partial x_j} + \rho u_j \frac{\partial \varphi}{\partial x_j} \right). \tag{2}$$

While the underlying physical equations are mathematically equivalent in an algebraic sense, the split-form is considerably more robust numerically when the equations are evaluated on a discrete mesh with finite-difference approximations [28]. The split-forms are computationally more expensive due to the increased number of floating-point operations required, however, as CFD codes are typically memory-bound, they are an efficient way of improving numerical stability for large-scale calculations at high Reynolds numbers. In this work, we apply the quadratic Blaisdell split-form [30] of the equations to improve numerical robustness throughout. As we are interested in the effect of low- and mixed-precision and the propagation of numerical errors in finite-difference approximations, other quadratic and cubic split-forms are also tested in the inviscid limit with varying numerical precision in Section 4.2.

### 3. Enabling mixed precision in OpenSBLI

# 3.1. Mixed precision using explicit finite difference methods

For simulation of transitional and turbulent compressible flows, in which a wide range of spatial and temporal scales are present, explicit finite difference schemes are commonly used. High-order finite differences are used for evaluating spatial derivatives, while low-storage variants of Runge-Kutta time advance schemes are adopted. The conservation form of the governing Navier-Stokes equations is used, with the vector of flow variables given by  $\mathbf{Q} = (\rho, \rho u, \rho v, \rho w, \rho E)^T$ , where  $\rho$  is the density, u, v, and w are the velocity components and  $E = e + (u^2 + v^2 + w^2)/2$  is the total energy per unit mass, adding the internal energy per unit mass e to the kinetic energy per unit mass. The complete governing equations are given in [31]. Here, we focus on the time advance step to explain how reduced precision schemes may be implemented.

The conservative flow variables are advanced in time using compact Runge-Kutta methods based on storage of Q and

$$Q_{DP,SP,HP}^{n+1} = Q_{DP,SP,HP}^{n} + \Delta t R_{DP,SP,HP}^{n}$$

$$Q = \begin{pmatrix} \rho \\ \rho u \\ \rho v \\ \rho w \\ \rho E \end{pmatrix}$$

$$n_{W} W_{DP,SP,HP}^{n}$$

$$Work arrays$$

Figure 1: Schematic of the use of  $n_W$  variable precision work arrays W to form residuals R for update of conservative variables Q during a typical Runge-Kutta substep (DP=double precision, SP=single precision, HP=half precision).

a change denoted  $\tilde{\mathbf{Q}}$ . At each substep *i* these storage locations are updated according to

$$\tilde{\mathbf{Q}}^{i} = A_{i}\tilde{\mathbf{Q}}^{i-1} + \Delta t \mathbf{R}^{i-1} \tag{3}$$

and

$$\mathbf{Q}^i = \mathbf{Q}^{i-1} + B_i \tilde{\mathbf{Q}}^i, \tag{4}$$

where  $A_i$  and  $B_i$  are scalar coefficients of the scheme,  $\Delta t$  is the time step and **R** is the residual, containing all the remaining terms from the governing equations. After m substeps the solution at the next time level n + 1 is given by

$$\mathbf{Q}^{n+1} = \mathbf{Q}^m. \tag{5}$$

The update procedure is shown schematically in Figure 1 based on a simple Euler update, but containing the essential features of equation 3. The residual  $\mathbf{R}$  needs to be computed from the solution  $\mathbf{Q}$  at the previous step. This step contains most of the computational cost of the algorithm and is typically accomplished using a number  $n_W$  of work arrays W, where  $n_W$  may be of the order of 20, but can be much more if curvilinear co-ordinates are used. The work arrays typically are the datasets containing first and second derivatives of various quantities which are eventually used to evaluate the residual,  $\mathbf{R}$ .

To discuss the use of mixed precision algorithms, we first note that each of the array types Q (flow variables), R (residuals) and W work arrays could in principle be represented using different numerical precision. A standard treatment would be to store all in double precision (denoted DP and shown in red in figure 1). One could in principle also do all the operations in single precision (SP, blue) or even half precision (HP, green). In this paper, we will also consider mixed precision cases; for example, a single/double mixed precision case (SPDP) can be defined where we retain **Q** in double precision, while using single precision for  $\mathbf{R}$  and all the W. Similarly, a half/single mixed precision case (HPSP) stores Q in single precision and R and W in half precision. Clearly, there are other options that we will discuss later. One could also split the residual R into different components that could be treated with different precision, as proposed in [32].

Two approaches to the work array usage are applied in this study. The first one is called the "default" method, and the second is called the "Storesome" method. The default method in OpenSBLI creates various 3D work arrays to calculate and store the residual terms in memory before passing them to the

main kernel that does the final evaluation of **R** involving the inviscid and viscous fluxes. This method is memory intensive, but helps with code structure and readability, mimicking what was previously done with manually-written code. The second method, called the "Storesome" method, only uses a few of the 3D work arrays and computes most of the derivatives directly within the kernel functions, as and when required. Jammy et al [33] demonstrated significant improvements with the Storesome approach, in terms of memory usage and run time.

#### 3.2. Generation of mixed-precision source codes using OpenS-BLI

The most recent version of OpenSBLI [23] was extended for this work to implement the different low- and mixed-precision algorithm strategies. This required the following changes to be made to the internal code-generation engine:

- A new user interface option in the high-level Python script for specification of the precision to be used globally within the simulation (double/single/half).
- Modifications to the array declaration types and input/output arguments to OPS parallel loops based on the selection made by the user.
- Explicit C/C++ casting of quantities appearing on the right-hand-side of equations in the simulation code, as required.
- A Python interface for specifying a lower/higher precision for certain array quantities (e.g. **Q**, **R**, **W** discussed in Section 3.1) to enable mixed-precision strategies.

The new interface for specifying lower- and mixed-precision is shown in the example code snippet below:

```
# Set the global simulation precision to single
SimulationDataType.set_datatype(FloatC)
# Define custom mixed-precision options using
    presets
mixed_precision_config = {
'q_vector' : ([], Double),
'RK_arrays' : ([], Double),
'residuals' : ([], FloatC),
'wk_arrays' : ([], FloatC),
                                                    8
'casting' : 'explicit'}
                                                    9
# Optionally, select custom arrays to set the
    precision of
custom_arrays = [block.location_dataset(dset) for 11
     dset in ['T', 'p']]
mixed_precision_config['custom'] = (custom_arrays 12
     Half)
# Call the OPS C code-generator
                                                    13
OPSC(alg, mixed_precision_config)
                                                    14
```

In line 2, the default global precision of the simulation is specified by the user as single (FloatC). A configuration dictionary is then created in lines 4-9 to specify mixed-precision alterations to the global precision depending on the storage quantity in question. Four presets are shown between lines 5-8, which, in this example, raise the precision of the conservative  $\mathbf{Q}$  and temporary Runge-Kutta  $\tilde{\mathbf{Q}}$  storage arrays to double precision. Other

available presets for residual  $\mathbf{R}$  and work-arrays  $\mathbf{W}$  are also shown. For completeness, a custom array option is also shown in lines 11-12. Here, the arrays for temperature and pressure (T,p) are set as half precision, to provide additional flexibility to explore more complex mixed-precision strategies. Finally, OpenSBLI's OPS C code-writer is called in line 14 with the requested mixed-precision configuration. Internally, the codegeneration engine will define the precision of these quantities and their API calls within the OPS library automatically based on the user input.

### 4. Results

# 4.1. Taylor Green test case

The Taylor-Green vortex problem has become a standard test case for assessing the accuracy and efficiency of schemes to solve the unsteady Navier-Stokes equations, particularly of high-order schemes [34]. It is a straightforward case to set up, consisting of a triply-periodic domain with a uniformly spaced grid and a prescribed analytic initial condition. From this starting condition, the flow evolves into discrete vortices which subsequently break down to a turbulent flow state. The kinetic energy of the initial condition eventually dissipates into heat and the accuracy of the method is assessed by monitoring the time evolution of the turbulence kinetic energy and the dissipation rate. Both incompressible and compressible forms of the problem can be specified. The effect of Mach number was demonstrated by Lusher & Sandham [31] and one of their cases was used for a 7-way multi-code comparison with a variety of numerical methodologies in [35].

The starting equations for the Taylor-Green vortex problem are given by

$$u(x, y, z, t = 0) = \sin(x)\cos(y)\cos(z), \tag{6}$$

$$v(x, y, z, t = 0) = -\cos(x)\sin(y)\cos(z),\tag{7}$$

$$w(x, y, z, t = 0) = 0, (8)$$

$$p(x, y, z, t = 0) = \frac{1}{\gamma M^2} + \frac{1}{16} \left[ \cos(2x) + \cos(2y) \right] \left[ 2 + \cos(2z) \right].$$
(9)

Here, M is the reference Mach number, while  $\gamma=1.4$  for air. The equations are solved in a non-dimensional form and all the quantities are non-dimensionalised with corresponding reference values. Also, the initial density  $\rho$  at the start of the simulations is evaluated based on the non-dimensional form of the equation of state, i.e.,

$$\rho(x, y, z, t = 0) = \gamma M^2 p.$$
 (10)

In the TGV problem, a constant initial reference temperature is assumed across the entire domain at the beginning at t=0, hence the non-dimensional temperature is equal to one and doesn't feature in Eq. 10.

All the simulations are carried out with fourth order central differencing. The solution domain size can be either a  $(2\pi)^3$ 

or (exploiting symmetries in the initial condition)  $\pi^3$ . Key parameters are the Reynolds and Mach numbers. For the tests of reduced precision, we adopt the triply symmetric case (denoted TGSym) that was part of the 2021 OpenSBLI release [9] with a Reynolds number set to Re = 800 to make the case better resolved on modest grids (compared to the Re = 1600 used in [35] requiring grids between 512<sup>3</sup> and 2048<sup>3</sup> for a supersonic case). A default resolution of 256<sup>3</sup> is adopted here, which is enough for these cases to be fully resolved (equivalent to 512<sup>3</sup> in a  $(2\pi)^3$  domain). Using an intermediate Mach number of M = 0.5 allows larger time steps and is more representative of compressible flow applications than the choice of M = 0.1that is commonly used to compare with incompressible simulations; however, we will also consider the effect of Mach number, since we wish to check for any issues in using reduced precision towards the incompressible limit. We also later consider an inviscid version of the problem to study the stability of various splitting schemes in the context of reduced precision algorithms.

Figure 2 shows a typical evolution of the flow field at a few different time instances. Contours of  $\rho E$  are shown for a M=0.5 TGV simulation run in double precision. The first frame (Fig. 2a) shows the smooth state of the flow at time t=0, as per the description in Eqs. 6-9. As time evolves, the evolution of the flow leads to the formation of smaller and smaller scale vortical structures (Figs. 2b and 2c), illustrating the cascade process of turbulent flow. With no production of turbulence, the flow (Fig. 2d) slowly decays.

Before we move to quantitative results, we outline the physical quantities of interest in the TGV problem to assess the efficacy of various precision calculations presented in this research. The volume-averaged kinetic energy at each instance of time is defined as

$$K = \frac{1}{V} \int_{V} \frac{1}{2} u_i u_i dV. \tag{11}$$

Here, V is the volume of the computational box and is equal to  $\pi^3$  for the symmetric case. We will also look at the evolution of solenoidal dissipation, which represents the enstrophy contribution to dissipation. The simulations performed in the present paper are all for subsonic Mach numbers where the dilatation part of dissipation is negligible. The equation for solenoidal dissipation is

$$\epsilon^{S} = \frac{1}{Re} \int_{V} \left( \epsilon_{ijk} \frac{\partial u_{k}}{\partial x_{i}} \right)^{2} dV. \tag{12}$$

Here, *Re* is the simulation Reynolds number, while the integrand represents the inner product of the vorticity vector, also known as enstrophy.

Figure 3 shows the behavior of K (left hand scale) and  $\epsilon^S$  (right hand scale) over a simulation time from t=0 to t=20. For spatially homogeneous decaying turbulence, the rate of change of K is proportional to  $-\epsilon$ , so the kinetic energy decays monotonically once small scale structures have formed and the dissipation, which is positive definite, becomes significant. Given the derivative nature of the relation between K and  $\epsilon$ , the solenoidal dissipation rate  $\epsilon^S$ , representing almost all of

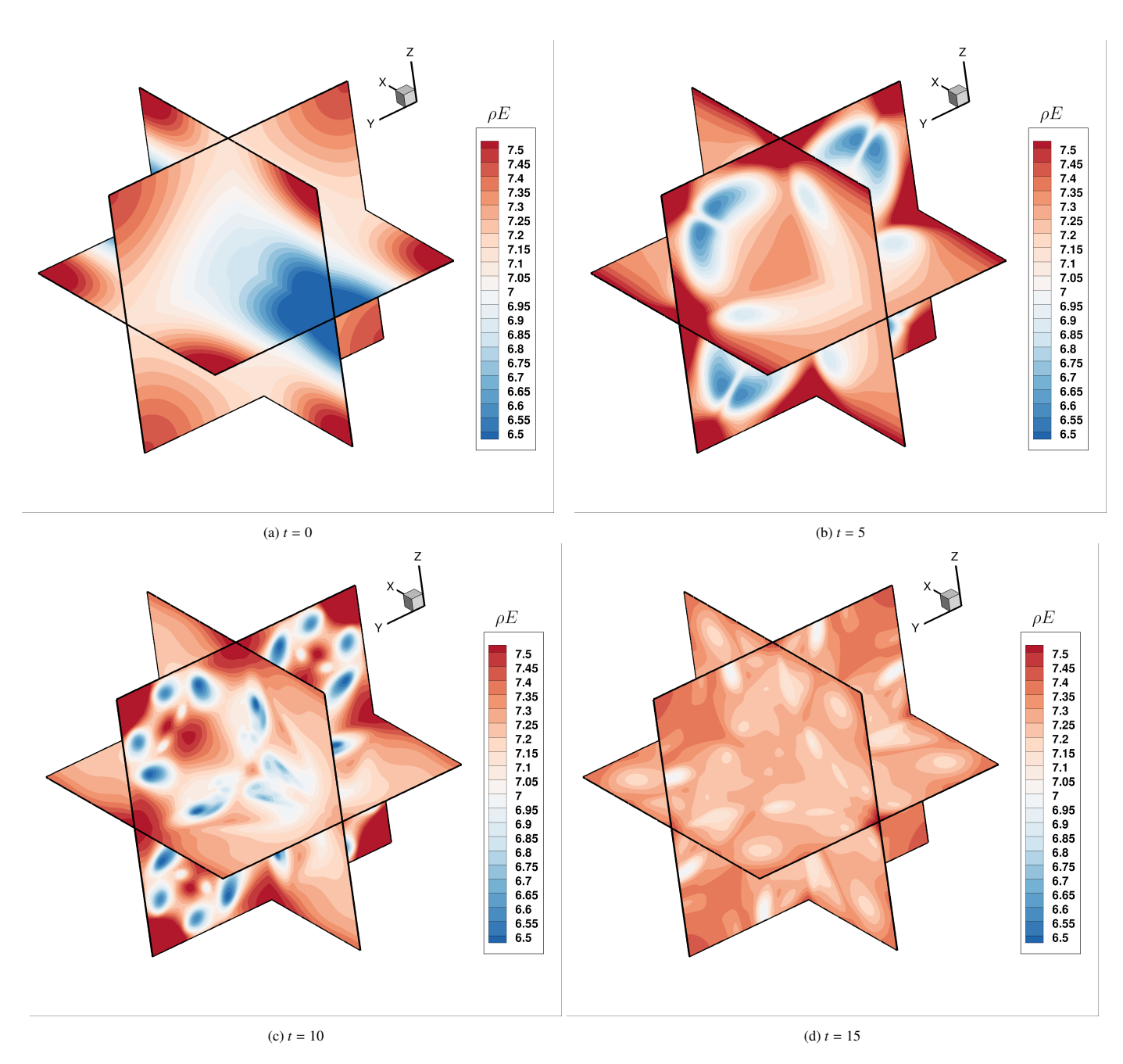


Figure 2: Contours of  $\rho E$  in three mutually perpendicular slices at the mid locations in x, y and z-directions, demonstrating the evolution of TGV state at different times: (a) t=0, (b) t=5, (c) t=10 and (d) t=15.

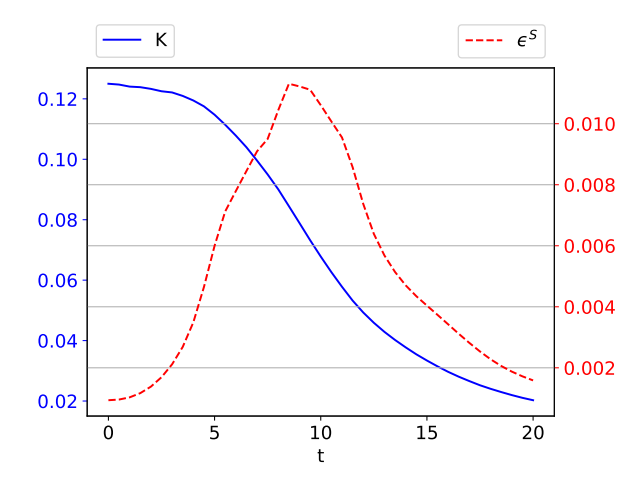


Figure 3: Kinetic energy (K) and dissipation ( $\epsilon^{S}$ ) relative to the time.

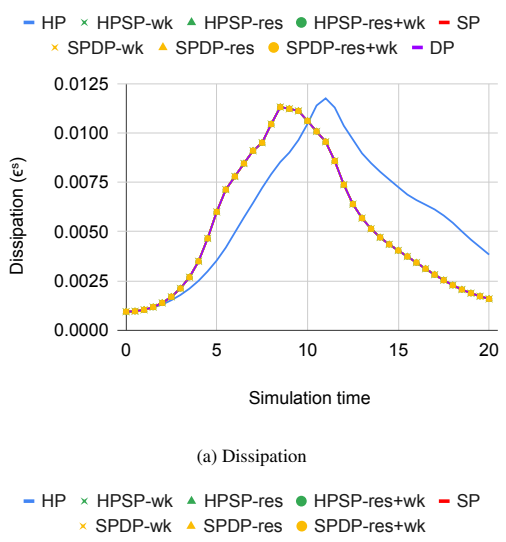
 $\epsilon$ , is a more sensitive measure of the numerical accuracy that is used to compare the different techniques employed in this study.

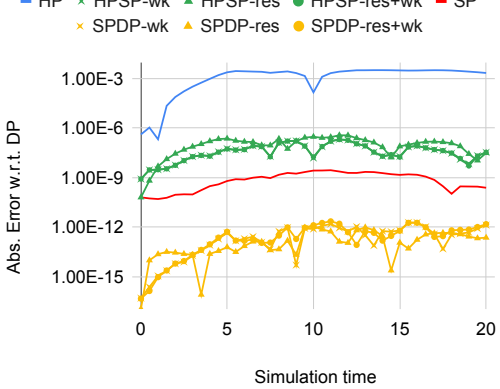
### 4.2. Accuracy

Figure 4a shows the effect of numerical precision on the behavior of the solenoidal dissipation rate as a function of time. Three standard versions are shown: HP using FP16 exclusively, SP using FP32, and DP using FP64. In addition, three kinds of mixed precision cases, namely '-wk', '-res', and '-res+wk', are presented between each pair of pure precisions. The '-wk' cases store only the work arrays in the lower precision, the '-res' cases store only the residual arrays in the lower precision, and the '-res+wk' cases store both the residual and work arrays in the lower precision. All test cases demonstrate overlapping results, with the exception of the FP16 version. The consistency observed among the other cases, with overlapping dissipation profiles, suggests comparable physical outcomes across these precision levels. Figure 4b presents a more detailed comparison and magnifies the differences by showing the absolute differences between each case and the highest precision run (FP64). The mixed-precision versions exhibit closer alignment with the higher precision of the two component precisions. Given the similarity in the observed error among the three mixed precision strategies, subsequent analyses will focus solely on the 'res+wk' strategy, as it offers the most significant computational speedup.

Figure 5 shows the state of TGV at t=10 for various types of precision computations. It is clear that the flow state is qualitatively the same for lower precision and mixed precision computations all the way to the HPSP mixed setup, when compared to the most accurate DP results presented in Fig. 2c. The results only deviate for the pure half-precision computations (HP), as can be noted from the last frame in the figure, where the vortex structures are more diffuse and sometimes in different locations.

The accuracy of the Storesome method is presented in Figure 6 in the same format as Figure 4. This method also demonstrates a high level of accuracy across different configurations, with the exception of the half-precision (FP16) run, which yielded inaccurate results. The overlapping results for





(b) Absolute difference of dissipation, compared to double precision

Figure 4: Numerical accuracy of TGsym app using different precision levels. Mesh size  $= 256^3$ , M = 0.5, Re = 800. The simulations were run for 8000 iterations using the default method.

all the other precision configurations indicate comparable physical outcomes. From Figure 6b, we can see how the levels of error varied among the mixed-precision runs. Notably, as the number of work arrays decreases significantly in the Storesome approach, a larger portion of the data is retained in higher precision. Consequently, a mixed half-single precision run exhibits a similar level of accuracy to that of a pure single precision run.

Figure 7 illustrates the impact of varying the timestep and Mach number M on the precision of the results. Small timesteps are required for low Mach number simulations and imply the additions of progressively smaller updates to the flow variables that are potentially sensitive to reduced precision. Here we separate out the effects of time step from those of Mach number. In Figure 7a, where the time step is varied while keeping the Mach number constant, it is evident that the reduced precision runs, where all variables are maintained at the same precision level (HP or SP), yield slightly less accurate results with smaller timesteps. However, when residuals and work arrays are set to lower precision, changes in timestep do not affect the results. This is because the Q array is retained in higher precision, allowing for more accurate result storage. All observed errors remain within a factor of 10 of the smallest representable num-

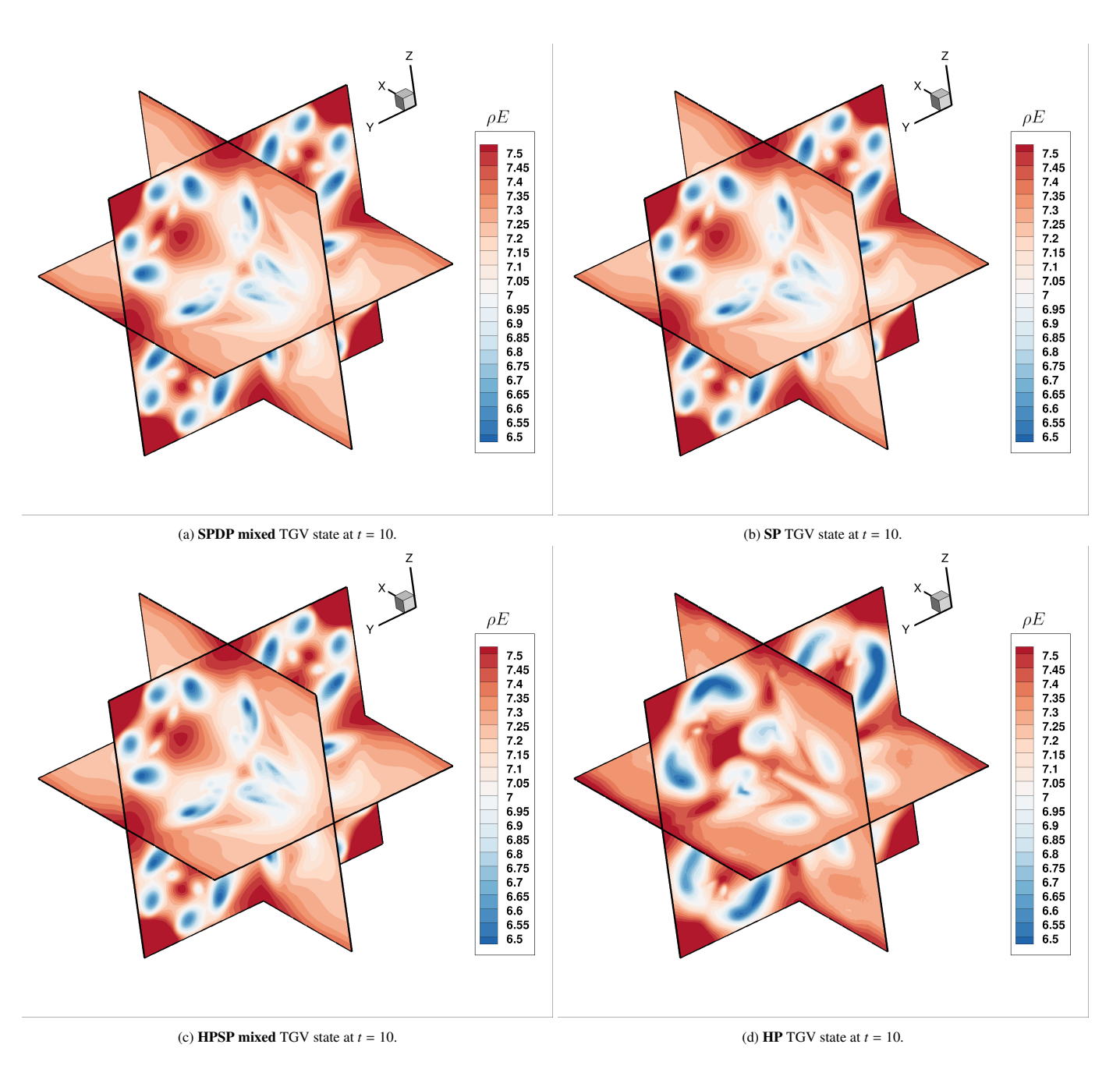
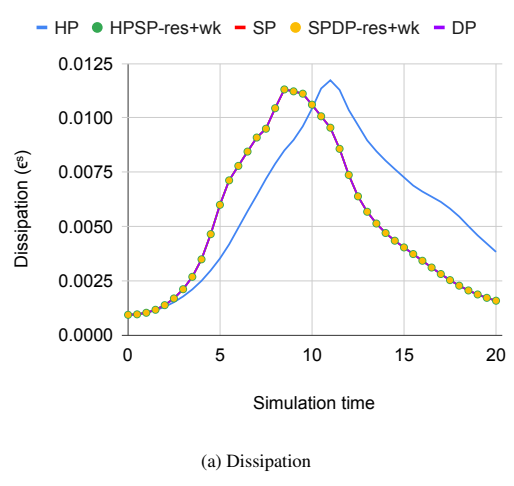
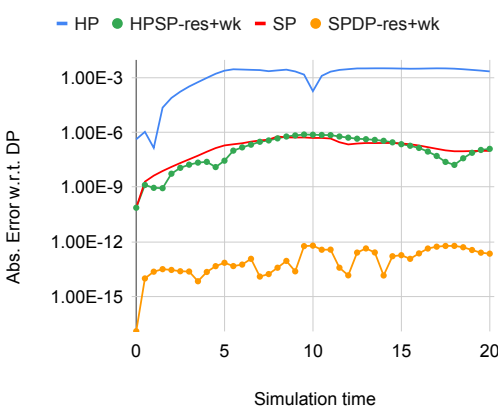


Figure 5: Contours of  $\rho E$  showing the TGV state at t = 10, close to the peak of dissipation: (a) SPDP, (b) SP, (c) HPSP and (d) HP.





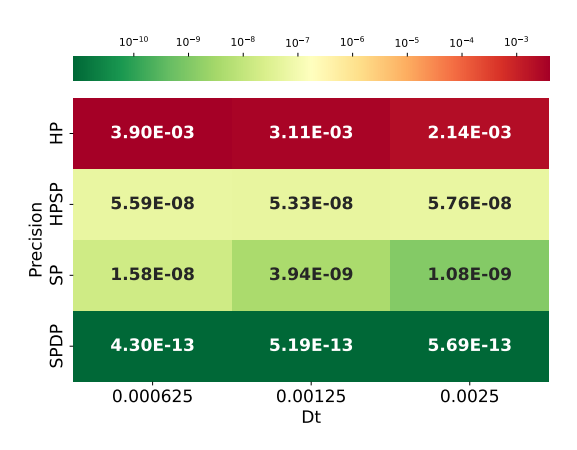
(b) Absolute difference of dissipation, compared to double precision

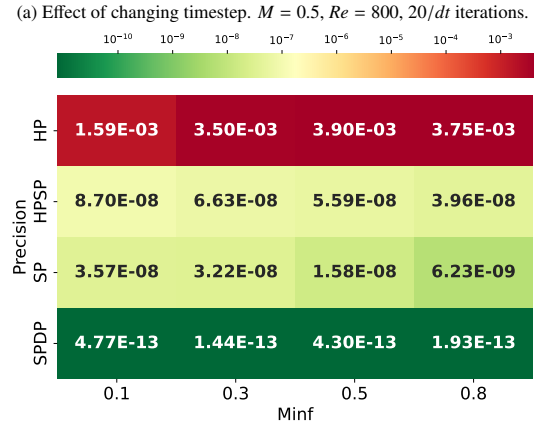
Figure 6: Numerical accuracy of TGsym app using different precision levels. Mesh size =  $256^3$ , M = 0.5, Re = 800. The simulations were run for 8000 iterations using the Storesome method.

ber for each specific precision. Figure 7b shows the effect of Mach number, while maintaining the same time step. While the HP case is incorrect for all Mach numbers, only a small increase in error is seen for the HPSP, SP, and SPDP cases as the Mach number is reduced. Overall, both subplots indicate that mixed/reduced precision runs can be effectively utilized.

We next consider a selection of the convective split-forms that are available in the OpenSBLI solver [23] to improve simulation robustness. As we have already observed that half precision does not produce consistent results for the TGV application (Figure 6), we limit the discussion here only to the HPSP algorithm compared to the full double precision (DP) result. A full list of the equations for each of the split forms is given in the appendix of [36]. In order to isolate the relationship between precision and split-formulation of the equations, this comparison is performed as an inviscid TGV calculation with the diffusive terms omitted. We use a coarsened  $N=64^3$  grid at  $M_{\infty}=0.4$  [36] to test the robustness of the split-forms at different numerical precisions.

Figure 8 shows the time evolution of global kinetic energy normalised by its initial value. For a robust numerical scheme, the normalised kinetic energy for the inviscid case should stay





(b) Effect of changing Mach number M. Re = 800, 32000 iterations, dt = 0.000625

Figure 7: The effect of changing parameters of the model on the numerical accuracy of TGsym app using different precision levels. Size=256³, default method. Values are the average of the absolute differences against the DP run of the dissipation at every 0.5 stepsize of simulation time.

at a value of one for as long as possible. The first thing to note in the figure is that, in the absence of physical viscosity in the inviscid limit considered here, several of the formulations (used for the convective terms of Navier-Stokes equations) diverge by showing exponential growth and eventually produce NaN when evaluated on a discrete mesh as non-linearities amplify aliasing errors. In particular, it can be observed that direct application of central differencing in the divergence form is unsuitable and the simulation rapidly diverges. Quadratic-split formulations by Blaisdell, Jameson, Kok, and Feiereisen (all listed in [36]) perform better, but still diverge within the standard simulation time used for Taylor-Green vortex problem (i.e. t = 20). In contrast, the cubic-split Kennedy-Gruber-Pirozzoli (KGP) [28] and Kinetic Energy and Entropy Preserving (KEEP) [36] schemes are robust and are able to maintain numerical stability even in the inviscid limit on a coarse grid. The physical behaviour we observe between the different split formulations is in good agreement with previous studies of this problem [36].

The effect of numerical precision is also shown on Figure 8, comparing double precision (solid line) with half-single precision (dashed line). Only very minor differences are observed between the full and mixed precision algorithms, with

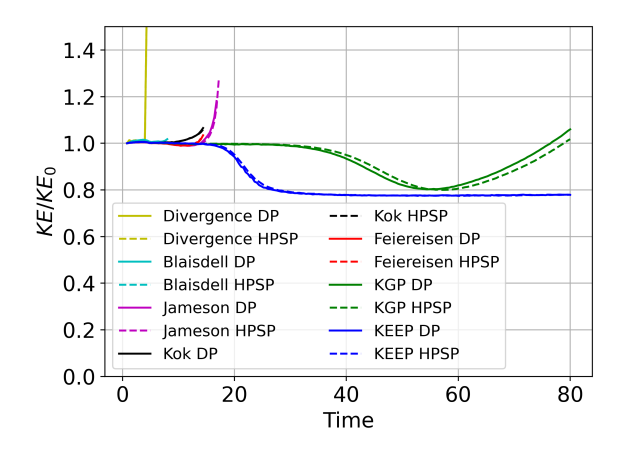


Figure 8: The effect of different split-forms on numerical accuracy of the inviscid Taylor-Green vortex application using DP and HPSP precision levels.  $N=64^3$  grid points,  $M_{\infty}=0.4$ , dt=0.004, inviscid calculation, StoreSome method.

the largest differences being observed for the KGP scheme [28]. In each case, the trends between the split forms are consistent between double and half-single precision. This demonstrates that the improved numerical robustness of split formulations for the convective terms of the Navier-Stokes equations persists even when applying reduced/mixed numerical precision. The benefits of the mixed precision strategies are maintained when using other formulations of the equations, and are therefore not limited to only the baseline split-form.

To conclude this section, we highlight the findings regarding the accuracy of mixed and half precision formats in our simulations. Our evaluations demonstrate that while mixed precision configurations, such as half-single precision (HPSP), maintain acceptable accuracy levels, pure half precision (HP) fails to meet the required standards across various conditions. Importantly, these results are consistent regardless of the simulation parameters, such as Reynolds number and Mach number, as well as the choice of numerical schemes. This reinforces the notion that while mixed precision techniques can be effectively employed in computational fluid dynamics (CFD) applications, careful selection of precision is crucial to ensure reliable outcomes. As we move forward in our research, understanding these accuracy implications will be essential for optimizing performance without compromising the integrity of simulation results.

# 4.3. Performance measurements

In the previous sections, we demonstrated how the usage of lower precision affects accuracy at the application level. In this subsection, we will examine the changes in performance and quantify the trade-offs involved. Under normal circumstances, a complete TGV simulation (mesh size =  $256^3 M = 0.5$ . Re = 800, 8000 iterations,  $\Delta t = 0.0025$ ) using FP64 precision on a GPU takes approximately 825.68 seconds. In contrast, we observed that the simulation rearranged according to the Storesome method is significantly faster, completing in just 402.48

seconds while utilizing nearly half as much memory. This efficiency allows us to conduct more or even larger simulations within given hardware constraints while ensuring that the final results remain qualitatively comparable. For the performance measurements, we retained the mesh size of 256<sup>3</sup> but ran the simulations for only 10% of the total time steps (i.e. to time t=2), executing each case five times and reporting the average of these runs. We then plotted the compute time per iteration, as this metric remains consistent throughout a simulation. Through our analysis of the representative TGV application, we illustrate what performance improvements users can expect in terms of both time and scale. For context, JAXA's aerofoil buffet applications run for three to four weeks using 120 Nvidia V100 GPUs [23, 25]. This highlights that running a substantial industrial application is not cheap; thus, any performance enhancement can be highly beneficial.

|      | Default   |         | Storesome |               |
|------|-----------|---------|-----------|---------------|
|      | runtime   | speedup | runtime   | speedup       |
| HP   | 42.43 ms  | 2.43 ×  | 18.67 ms  | 2.69 ×        |
| HPSP | 47.71 ms  | 2.16 ×  | 22.13 ms  | $2.27 \times$ |
| SP   | 56.95 ms  | 1.81 ×  | 25.00 ms  | $2.01 \times$ |
| SPDP | 74.02 ms  | 1.39 ×  | 37.60 ms  | $1.34 \times$ |
| DP   | 103.21 ms | 1.00 ×  | 50.31 ms  | $1.00 \times$ |

Table 1: Runtime per iteration and speedup compared to the double precision run time of the TGsym app are shown for the default and storesome generation methods. Mesh size= $256^3$ , M=0.5, Re=800, 800 iterations. The measurements are performed on a single NVIDIA A100-SXM4-40GB GPU with an AMD EPYC<sup>TM</sup> 7763 (Milan) CPU.

|      | Default   |         | Storesome |               |
|------|-----------|---------|-----------|---------------|
|      | runtime   | speedup | runtime   | speedup       |
| HP   | 75.09 ms  | 2.31 ×  | 33.90 ms  | 3.00 ×        |
| HPSP | 90.23 ms  | 1.92 ×  | 48.65 ms  | $2.09 \times$ |
| SP   | 108.91 ms | 1.59 ×  | 53.84 ms  | $1.89 \times$ |
| SPDP | 140.69 ms | 1.23 ×  | 92.51 ms  | $1.10 \times$ |
| DP   | 173.60 ms | 1.00 ×  | 101.68 ms | $1.00 \times$ |

Table 2: Runtime per iteration and speedup compared to the double precision run time of the TGsym app are shown for the default and storesome generation methods. Mesh size= $256^3$ , M = 0.5, Re=800, 800 iterations. The measurements are performed on a single AMD MI250X GPU with a 64-core AMD Trento CPU.

The performance evaluation of the TGsym application, shown in Table 1 and Table 2, reveals significant differences in runtime and speedup across various precision techniques on multiple GPU platforms. It is important to note that the Storesome method, by design, uses significantly fewer data arrays compared to the default method. This inherent efficiency of the Storesome approach contributes to its faster runtime performance by default.

As we transition to lower precision methods, we observe a consistent increase in speedup. However, the approximate doubling of speedup ceases when using half precision (FP16). Currently, OPS does not support packed half precision types, such as half2, meaning that instruction throughput is still as

if we were using FP32, and only the memory movement is reduced. The mixed precision configurations, specifically HPSP and SPDP, strike a balance between performance and accuracy, yielding speedups that fall between their respective pure precision counterparts (HP/SP and SP/DP).

On the NVIDIA A100 GPU, the mixed precision strategies generally achieve notable speedups due to native support for half precision arithmetic. Similarly, the AMD MI250X GPU, which also features native FP16 hardware support, benefits from mixed precision configurations, offering enhanced performance by leveraging its FP16 capabilities.

|      | Default   |               | Storesome |               |
|------|-----------|---------------|-----------|---------------|
|      | runtime   | speedup       | runtime   | speedup       |
| HP   | 68.48 ms  | 5.71 ×        | 21.39 ms  | 8.12 ×        |
| HPSP | 105.22 ms | $3.71 \times$ | 47.31 ms  | $3.67 \times$ |
| SP   | 185.23 ms | 2.11 ×        | 65.05 ms  | $2.67 \times$ |
| SPDP | 249.11 ms | $1.57 \times$ | 123.22 ms | $1.41 \times$ |
| DP   | 390.71 ms | 1.00 ×        | 173.68 ms | $1.00 \times$ |

Table 3: Runtime per iteration and speedup compared to the double precision run of the TGsym app using the default and Storesome generation methods. Mesh size=256<sup>3</sup>, M=0.5, Re=800, 800 iterations. The measurements are performed on Intel Xeon Platinum 8592+ CPU

|             | Default   |               | Storesome |               |
|-------------|-----------|---------------|-----------|---------------|
|             | runtime   | speedup       | runtime   | speedup       |
| HP          | 78.78 ms  | 4.48 ×        | 47.76 ms  | 2.80 ×        |
| <b>HPSP</b> | 107.09 ms | $3.30 \times$ | 48.71 ms  | $2.74 \times$ |
| SP          | 169.90 ms | $2.08 \times$ | 63.48 ms  | $2.10 \times$ |
| SPDP        | 228.69 ms | 1.54 ×        | 105.17 ms | $1.27 \times$ |
| DP          | 353.32 ms | $1.00 \times$ | 133.49 ms | $1.00 \times$ |

Table 4: Runtime per iteration and speedup compared to the double precision run of the TGsym app using the default and Storesome generation methods. Mesh size=256<sup>3</sup>, M=0.5, Re=800, 800 iterations. The measurements are performed on AMD EPYC Genoa (4th Gen) CPU

|      | Default    |               | Storesome  |               |
|------|------------|---------------|------------|---------------|
|      | runtime    | speedup       | runtime    | speedup       |
| HP   | 772.73 ms  | 3.91 ×        | 312.46 ms  | 4.18 ×        |
| HPSP | 1021.08 ms | $2.96 \times$ | 524.46 ms  | $2.49 \times$ |
| SP   | 1536.12 ms | $1.97 \times$ | 616.89 ms  | $2.12 \times$ |
| SPDP | 2013.77 ms | $1.50 \times$ | 1006.87 ms | $1.30 \times$ |
| DP   | 3020.79 ms | $1.00 \times$ | 1306.43 ms | $1.00 \times$ |

Table 5: Runtime per iteration and speedup compared to the double precision run of the TGsym app using the default and Storesome generation methods. Mesh size=512<sup>3</sup>, M=0.5, Re=800, 800 iterations. The measurements are performed on Intel Xeon Platinum 8592+ CPU

Table 3 presents the performance of various methods on an Intel CPU platform. Unlike the GPU, this CPU utilizes fixed 512-bit wide vectors, allowing it to fully utilize these vectors with smaller data sizes thanks to compiler auto-vectorization. As a result, we observe the expected doubling of speedup even when employing FP16 precision. Additionally, the data indicates superlinear scaling, which occurs as more data fits into

the cache memory. In contrast, Table 4 shows that on an AMD CPU, which lacks FP16 vector optimizations, the performance does not improve significantly for HPSP and HP precision runs. Furthermore, Table 5 demonstrates that with a larger mesh size that exceeds cache capacity, the speedup approaches the expected 4x, thereby validating the superlinear speedup observed with the original mesh size.

|      | Default |               | Storesome |               |
|------|---------|---------------|-----------|---------------|
|      | Memory  | Gain          | Memory    | gain          |
| HP   | 2.21 GB | 4.00 ×        | 1.09 GB   | 4.00 ×        |
| HPSP | 2.72 GB | $3.25 \times$ | 1.60 GB   | $2.72 \times$ |
| SP   | 4.41 GB | $2.00 \times$ | 2.17 GB   | $2.00 \times$ |
| SPDP | 5.43 GB | $1.63 \times$ | 3.19 GB   | $1.36 \times$ |
| DP   | 8.83 GB | 1.00 ×        | 4.35 GB   | $1.00 \times$ |

Table 6: Memory used with the TGsym app and memory gain compared to the double precision run. Size=256<sup>3</sup>.

Table 6 presents the memory consumption associated with each configuration. All mixed precision cases fall between the memory requirements of their respective pure precision counterparts. The degree to which data arrays are cast to lower precision directly influences the overall memory savings. For instance, when fewer arrays are converted, as seen with the Storesome method, the resulting memory savings are less pronounced, as are the resulting speedups. Overall, reducing an application's memory footprint enables the accommodation of larger problems within the same hardware constraints. For example, by halving the data size in an application that fully utilizes a GPU's memory, we can effectively double the overall mesh size. This capability is crucial for improving computational efficiency and expanding the scope of solvable problems in high-performance computing environments.

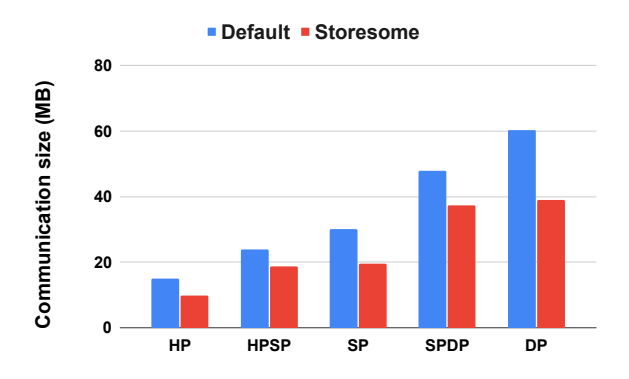
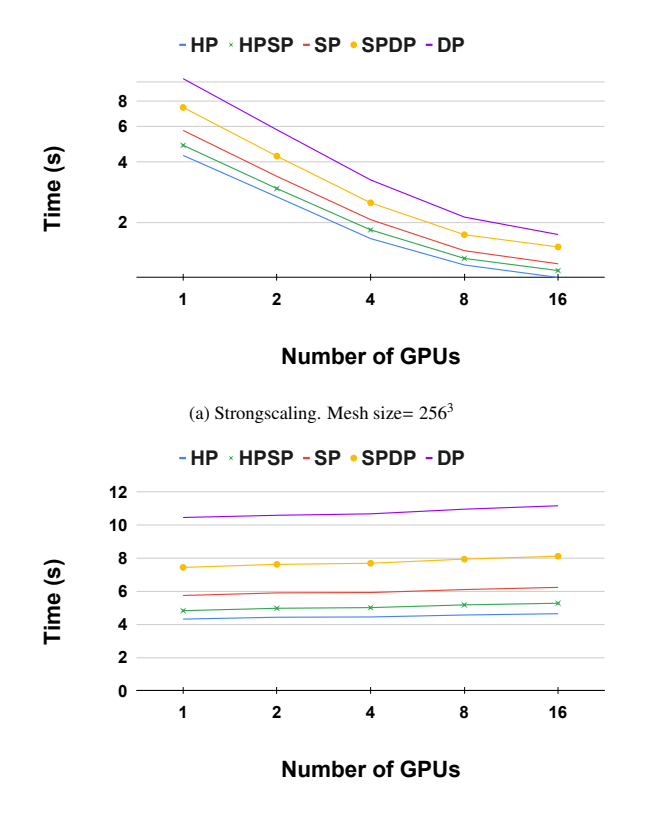


Figure 9: Average volume of MPI communications per process per iteration on the TGsym app, using 4 MPI processes. Size=256<sup>3</sup>

Figure 9 illustrates the communication requirements associated with utilizing multiple MPI processes. It is important to note that inter-node communication (usually through Infiniband) can be significantly slower than intra-node communication (usually through NVLink). Consequently, the reduction in data sizes has a pronounced effect on speedup when scaling across multiple devices. This figure also emphasizes the impact of selecting arrays to use in lower precision during mixed



(b) Weakscaling, Mesh size= 256<sup>3</sup>, multiplied by the number of processes in X direction

Figure 10: Strong- and weakscaling of the TGsym app with GPUdirect using different precision levels. M=0.5, Re=800, 8000 iterations.

configurations. Since work arrays are communicated less frequently than other state arrays and the Storesome method utilizes fewer work arrays, the result is that mixed setups do not substantially reduce the MPI communication volume when employing the Storesome approach.

Figure 10 illustrates both the strong and weak scaling performance of the TGsym application across different precision levels. As anticipated, all configurations demonstrate effective scaling behavior. The parallel efficiency results from the strong scaling measurements indicate effective scalability across all precision configurations, with efficiencies ranging from 90% to 25% as the number of processes increases. It is important to note that at higher process counts, message latency has a more significant impact on performance than message size. As the number of processes increases, the number of messages per process remains constant (and even slightly increases); however, the sizes of these messages decrease. This reduction in message size helps explain why double precision (DP) performance approaches that of single precision (SP) in these scenarios. In contrast, the weak scaling measurements reveal consistently high efficiencies across all configurations, exceeding 92%. This indicates that the TGsym application scales exceptionally well, irrespective of the precision level used.

#### 5. Conclusions and Future Work

In this paper, we have explored the implementation and effectiveness of mixed precision techniques in compressible turbulent flow simulations using explicit finite difference schemes. By extending both the OPS library and the OpenSBLI framework to support mixed precision arithmetic, we demonstrated that significant performance gains can be achieved without sacrificing numerical accuracy, provided that the precision is selected carefully. Our experiments using the Taylor-Green vortex benchmark revealed that while reduced precision formats such as single and mixed half-single precision yield acceptable results, pure half-precision computations suffer from unacceptable numerical inaccuracies.

The proposed mixed precision algorithm effectively balances performance and precision, allowing for improved computational efficiency, particularly in memory usage and communication overheads, which are crucial in multi-CPU and multi-GPU environments. Our analysis indicates that mixed precision approaches can provide substantial speedups, especially in larger-scale simulations, without compromising the integrity of the results.

Several avenues remain for further exploration:

- Larger and More Complex Applications: To fully understand the potential of mixed precision techniques, future work will experiment with multi-block airfoils, with opportunities to use different precisions on different blocks, and shock-capturing schemes, in which some shock-capturing algorithms will need to be adjusted for reduced precision. These experiments will also help assess the scalability and generalizability of our methods in real-world, high-performance computing (HPC) environments.
- Improving Half-Precision Performance: Since pure half-precision (FP16) simulations did not yield acceptable accuracy in our current tests, we did not prioritize optimizing FP16 performance in this work. However, there may be specific simulations where FP16 can produce satisfactory results, particularly on GPU architectures. To support these scenarios, future work will focus on enhancing OPS to define global constants in half-precision and to utilize packed types, allowing multiple half-precision calculations within a single warp. These optimizations could unlock further performance gains on hardware optimized for FP16 computations, such as modern GPUs.
- As well as the possibility to treat different terms (for example viscous terms) with different precision, as noted in the introduction, it is also interesting to consider whether the precision can be adjusted in an adaptive way, for example in an analogous manner to adaptive mesh refinement, where the mesh is refined based on local error criteria.

By addressing these areas, we aim to further optimize the trade-offs between computational efficiency and numerical accuracy, thereby pushing the boundaries of what is possible with mixed precision in large-scale turbulent simulations.

# Acknowledgements

This research was supported by the National Research, Development and Innovation Fund of Hungary (FK 145931), under the FK\_23 funding scheme. We acknowledge KIFÜ (Governmental Agency for IT Development, Hungary, https://ror.org/01s0v4q65) for awarding us access to the Komondor HPC facility based in Hungary. NDS and PKS acknowledge the support of EPSRC under grant EP/W026686/1. DJL and the development of OpenSBLI V3.0 were supported by the Japan Society for the Promotion of Science (JSPS) under grant 22F22059. We are grateful for the support of the OneAPI Innovator program, and the advice and assistance of Rupak Roy, Omar Toral, Sri Ramkrishna at Intel in particular.

# Declaration of generative AI and AI-assisted technologies in the writing process.

During the preparation of this work, the author(s) utilized both the Perplexity AI tool and ChatGPT to assist primarily in writing and phrasing, enhancing the overall flow of the text for better readability. After employing these tools, the author(s) reviewed and edited the material as necessary and take(s) full responsibility for the content of the published article.

#### References

- J. Sun, G. D. Peterson, O. O. Storaasli, High-performance mixedprecision linear solver for fpgas, IEEE Transactions on Computers 57 (12) (2008) 1614–1623. doi:10.1109/TC.2008.89.
- [2] A. Abdelfattah, S. Tomov, J. Dongarra, Towards half-precision computation for complex matrices: A case study for mixed precision solvers on gpus, in: 2019 IEEE/ACM 10th Workshop on Latest Advances in Scalable Algorithms for Large-Scale Systems (ScalA), 2019, pp. 17–24. doi:10.1109/ScalA49573.2019.00008.
- [3] J. D. Hogg, J. A. Scott, A fast and robust mixed-precision solver for the solution of sparse symmetric linear systems, ACM Trans. Math. Softw. 37 (2) (apr 2010). doi:10.1145/1731022.1731027. URL https://doi.org/10.1145/1731022.1731027
- [4] N. J. Higham, T. Mary, Mixed precision algorithms in numerical linear algebra, Acta Numerica 31 (2022) 347–414. doi:10.1017/S0962492922000022.
- [5] P. Luszczek, A. Abdelfattah, H. Anzt, A. Suzuki, S. Tomov, Batched sparse and mixed-precision linear algebra interface for efficient use of gpu hardware accelerators in scientific applications, Future Generation Computer Systems 160 (2024) 359–374. doi:https://doi.org/10. 1016/j.future.2024.06.004. URL https://www.sciencedirect.com/science/article/pii/
- [6] A. Abdelfattah, H. Anzt, A. Ayala, E. G. Boman, E. C. Carson, S. Cayrols, T. Cojean, J. J. Dongarra, R. Falgout, M. Gates, T. Grutzmacher, N. J. Higham, S. E. Kruger, S. Li, N. Lindquist, Y. Liu, J. A. Loe, P. Nayak, D. Osei-Kuffuor, S. Pranesh, S. Rajamanickam, T. Ribizel, B. B. Smith, K. Swirydowicz, S. J. Thomas, S. Tomov, Y. M. Tsai, I. Yamazaki, U. M. Yang, Advances in mixed precision algorithms: 2021 edition (8 2021). doi:10.2172/1814447.
  - URL https://www.osti.gov/biblio/1814447

S0167739X24003017

- [7] M. Lehmann, M. J. Krause, G. Amati, M. Sega, J. Harting, S. Gekle, Accuracy and performance of the lattice boltzmann method with 64-bit, 32-bit, and customized 16-bit number formats, Phys. Rev. E 106 (2022) 015308. doi:10.1103/PhysRevE.106.015308. URL https://link.aps.org/doi/10.1103/PhysRevE.106. 015308
- [8] F. Brogi, S. Bnà, G. Boga, G. Amati, T. Esposti Ongaro, M. Cerminara, On floating point precision in computational fluid dynamics using openfoam, Future Generation Computer Systems 152 (2024) 1-16. doi:https://doi.org/10.1016/j.future.2023.10.006. URL https://www.sciencedirect.com/science/article/pii/S0167739X23003813
- [9] D. J. Lusher, S. P. Jammy, N. D. Sandham, OpenSBLI: Automated codegeneration for heterogeneous computing architectures applied to compressible fluid dynamics on structured grids, Computer Physics Communications 267 (2021) 108063. doi:https://doi.org/10.1016/j. cpc.2021.108063.
- [10] I. Z. Reguly, G. R. Mudalige, M. B. Giles, Loop Tiling in Large-Scale Stencil Codes at Run-Time with OPS, IEEE Transactions on Parallel and Distributed Systems 29 (4) (2018) 873–886. doi:10.1109/TPDS. 2017.2778161.
- [11] Ieee standard for floating-point arithmetic, IEEE Std 754-2019 (Revision of IEEE 754-2008) (2019) 1-84doi:10.1109/IEEESTD.2019. 8766229.
- [12] E. Goubault, Static analyses of the precision of floating-point operations, in: P. Cousot (Ed.), Static Analysis, Springer Berlin Heidelberg, Berlin, Heidelberg, 2001, pp. 234–259.
- [13] F. Benz, A. Hildebrandt, S. Hack, A dynamic program analysis to find floating-point accuracy problems, SIGPLAN Not. 47 (6) (2012) 453–462. doi:10.1145/2345156.2254118. URL https://doi.org/10.1145/2345156.2254118
- [14] A. Haidar, S. Tomov, J. Dongarra, N. J. Higham, Harnessing gpu tensor cores for fast fp16 arithmetic to speed up mixed-precision iterative refinement solvers, in: SC18: International Conference for High Performance Computing, Networking, Storage and Analysis, 2018, pp. 603–613. doi:10.1109/SC.2018.00050.
- [15] J. Wan, W. Wang, Z. Zhang, Enhancing computational efficiency in 3d seismic modelling with half-precision floating-point numbers based on the curvilinear grid finite-difference method, Geophysical Journal International (2024).
  - URL https://api.semanticscholar.org/CorpusID:271042153
- [16] P. Luszczek, I. Yamazaki, J. Dongarra, Increasing accuracy of iterative refinement in limited floating-point arithmetic on half-precision accelerators, in: 2019 IEEE High Performance Extreme Computing Conference (HPEC), 2019, pp. 1–6. doi:10.1109/HPEC.2019.8916392.
- [17] Intel, Bfloat16 hardware numerics definition, https://www.intel.com/content/dam/develop/external/us/en/documents/bf16-hardware-numerics-definition-white-paper.pdf (November 2018).
- [18] Y. Tortorella, L. Bertaccini, L. Benini, D. Rossi, F. Conti, Redmule: A mixed-precision matrix—matrix operation engine for flexible and energy-efficient on-chip linear algebra and tinyml training acceleration, Future Generation Computer Systems 149 (2023) 122-135. doi:https://doi.org/10.1016/j.future.2023.07.002. URL https://www.sciencedirect.com/science/article/pii/S0167739X23002546
- [19] I. Ober, I. Ober, On Patterns of Multi-domain Interaction for Scientific Software Development focused on Separation of Concerns, Procedia Computer Science 108 (2017) 2298–2302.
- [20] C. T. Jacobs, S. P. Jammy, N. D. Sandham, OpenSBLI: A framework for the automated derivation and parallel execution of finite difference solvers on a range of computer architectures, Journal of Computational Science 18 (2017) 12 – 23.
- [21] D. J. Lusher, S. P. Jammy, N. D. Sandham, Shock-wave/boundary-layer interactions in the automatic source-code generation framework opensbli, Computers & Fluids 173 (2018) 17 – 21.
- [22] D. J. Lusher, G. N. Coleman, Numerical study of compressible wall-bounded turbulence the effect of thermal wall conditions on the turbulent Prandtl number in the low-supersonic regime, International Journal of Computational Fluid Dynamics 36 (9) (2022) 797–815.
- [23] D. J. Lusher, A. Sansica, N. D. Sandham, J. Meng, B. Siklósi,

- A. Hashimoto, OpenSBLI v3.0: High-fidelity multi-block transonic aerofoil CFD simulations using domain specific languages on GPUs, Computer Physics Communications 307 (2025) 109406. doi:https://doi.org/10.1016/j.cpc.2024.109406.
- [24] D. J. Lusher, A. Sansica, A. Hashimoto, Effect of Tripping and Domain Width on Transonic Buffet on Periodic NASA-CRM Airfoils, AIAA Journal (2024) 1–20.
- [25] D. J. Lusher, A. Sansica, A. Hashimoto, Implicit large eddy simulations of three-dimensional turbulent transonic buffet on wide-span infinite wings, Journal of Fluid Mechanics 1007 (2025) A26. doi:10.1017/ifm.2025.48
- [26] S. Pirozzoli, Numerical Methods for High-Speed Flows, Annual Review of Fluid Mechanics 43 (1) (2011) 163–194.
- [27] G. Coppola, F. Capuano, L. de Luca, Discrete Energy-Conservation Properties in the Numerical Simulation of the Navier–Stokes Equations, Applied Mechanics Reviews 71 (1), 010803 (03 2019).
- [28] G. Coppola, F. Capuano, S. Pirozzoli, L. de Luca, Numerically stable formulations of convective terms for turbulent compressible flows, Journal of Computational Physics 382 (2019) 86–104.
- [29] W. J. Feiereisen, W. C. Reynolds, J. H. Ferziger, Numerical simulation of a compressible homogeneous, turbulent shear flow. ph.d. thesis, 1981. URL https://ntrs.nasa.gov/citations/19820003523
- [30] G. Blaisdell, E. Spyropoulos, J. Qin, The effect of the formulation of nonlinear terms on aliasing errors in spectral methods, Applied Numerical Mathematics 21 (3) (1996) 207–219. doi:https://doi.org/10. 1016/0168-9274(96)00005-0.
- [31] D. J. Lusher, N. D. Sandham, Assessment of Low-Dissipative Shock-Capturing Schemes for the Compressible Taylor-Green Vortex, AIAA Journal 59 (2) (2020) 533–545. doi:10.2514/1.J059672.
- [32] P. Schlatter, M. Karp, R. Stanly, H. Song, T. Mukha, L. Galimberti, S. Toosi, M. Münsch, L. Dalcin, S. Rezaeiravesh, N. Jansson, S. Markidis, M. Parsani, S. T. Bose, S. K. Lele, Impact of low floating-point precision on high-fidelity simulations of turbulence, in: 77th Annual Meeting of the Division of Fluid Dynamics, American Physical Society, 2024, presented at 77th Annual Meeting of the Division of Fluid Dynamics, APS, Chair: Adrian Lozano-Duran, Caltech / MIT. URL https://meetings.aps.org/Meeting/DFD24/Session/B37.6
- [33] S. P. Jammy, C. T. Jacobs, N. D. Sandham, Performance evaluation of explicit finite difference algorithms with varying amounts of computational and memory intensity, Journal of Computational Science 36 (2019) 100565. doi:https://doi.org/10.1016/j.jocs.2016.10.015. URL https://www.sciencedirect.com/science/article/pii/ S1877750316302708
- [34] J. DeBonis, Solutions of the Taylor-Green Vortex Problem Using High-Resolution Explicit Finite Difference Methods, in: 51st AIAA Aerospace Sciences Meeting including the New Horizons Forum and Aerospace Exposition, Aerospace Sciences Meetings, American Institute of Aeronautics and Astronautics, 2013.
- [35] J.-B. Chapelier, D. J. Lusher, W. Van Noordt, C. Wenzel, T. Gibis, P. Mossier, A. Beck, G. Lodato, C. Brehm, M. Ruggeri, C. Scalo, N. Sandham, Comparison of high-order numerical methodologies for the simulation of the supersonic Taylor–Green vortex flow, Physics of Fluids 36 (5) (2024) 055146. doi:10.1063/5.0206359.
- [36] Y. Kuya, K. Totani, S. Kawai, Kinetic energy and entropy preserving schemes for compressible flows by split convective forms, Journal of Computational Physics 375 (2018) 823-853. doi:https://doi.org/ 10.1016/j.jcp.2018.08.058.